Heliyon 5 (2019) e02766

Contents lists available at ScienceDirect

Heliyon

journal homepage: www.heliyon.com

Heliyon

Research article

Physicochemical characteristics and photocatalytic performance of TiO_2/SiO_2 catalyst synthesized using biogenic silica from bamboo leaves

Is Fatimah [a,*], Nurcahyo Iman Prakoso [a], Imam Sahroni [a], M. Miqdam Musawwa [a], Yoke-Leng Sim [b], Fethi Kooli [c], Oki Muraza [d]

[a] Chemistry Department, Universitas Islam Indonesia, Kampus Terpadu UII, Jl. Kaliurang Km 14, Sleman, Yogyakarta, Indonesia
[b] Chemistry Department, Universiti Tunku Abdul Rahman, Perak, Malaysia
[c] Taibah University-Al Mahd Branch, Community College- Al-Mahd, 44412, Saudi Arabia
[d] King Fahd University of Petroleum & Minerals, Dhahran, 31261, Saudi Arabia

ARTICLE INFO

Keywords:
Materials chemistry
Environmental science
TiO2/SiO2 composites
Photocatalyst
Biogenic silica
TiO2

ABSTRACT

In this work, TiO_2/SiO_2 composite photocatalysts were prepared using biogenic silica extracted from bamboo leaves and titanium tetraisopropoxide as a titania precursor via a sol–gel mechanism. A study of the physicochemical properties of materials as a function of their titanium dioxide content was conducted using Fourier transform infrared spectroscopy, a scanning electron microscope, a diffuse reflectance ultraviolet-visible (UV-vis) spectrophotometer, and a gas sorption analyzer. The relationship between physicochemical parameters and photocatalytic performance was evaluated using the methylene blue (MB) photocatalytic degradation process under UV irradiation with and without the addition of H_2O_2 as an oxidant. The results demonstrated that increasing the TiO_2 helps enhance the parameters of specific surface area, the pore volume, and the particle size of titanium dioxide, while the band gap energy reaches a maximum of 3.21 eV for 40% and 60% Ti content. The composites exhibit photocatalytic activity with the MB degradation with increasing photocatalytic efficiency since the composites with 40 and 60% wt. of TiO_2 demonstrated the higher degradation rate compared with TiO_2 in the presence and absence of H_2O_2. This higher rate is correlated with the higher specific surface area and band gap energy compared with those of TiO_2.

1. Introduction

Environmental remediation technology is the one of the most studied topics in environmental science, as there are many pollutants with varying characteristics produced by a wide range of industrial activities. Advanced oxidation processes involving photocatalytic mechanisms (photo-oxidation, photoreduction, and photodegradation) are techniques that have attracted attention during the five decades since they were introduced by Fujishima and Honda in 1970. Photocatalytic oxidation is a promising method for the environmentally safe degradation of organic wastewater, including dye waste from the textile industry [1, 2]. In addition to being a renewable process, the photocatalytic oxidation of dyes and organic molecules carries a lower cost compared to other techniques, such as adsorption, chemical oxidation, and ozonation [3, 4, 5].

This technique is highly regarded due to its use of photons from solar energy, the lack of chemicals, and the low cost. Highly active photocatalysts are a requirement, and TiO_2 is a very well-known photocatalyst material [5, 6] However, some modification of TiO_2 is required to enhance its performance for industrial applications. In addition to doping and the structural modification of titania nanoparticles to change the photocatalytic properties, supported titania has been reported to exhibit a different photocatalytic performance from that of titania alone [8, 9, 10]. The support material gives better results due to its interaction with titanium oxide. Therefore, titania-silica (TiO_2/SiO_2) composite is the most well-known and intensively studied material [11, 12, 13, 14]. Silica-supported titanium oxide exhibits a different photocatalytic performance than titania alone [7, 8, 9, 10]. This is partly because of the interaction between titanium oxide and silica and partly because of the different structures of surface titanate and bulk titania. Some studies have revealed a relationship between a material's photocatalytic activity and the surface titanium oxide structure, preparation method, and loading amount. To improve the stability and other properties of TiO_2/SiO_2, a recent approach to TiO_2/SiO_2 synthesis was developed that

* Corresponding author.
E-mail address: isfatimah@uii.ac.id (I. Fatimah).

https://doi.org/10.1016/j.heliyon.2019.e02766
Received 5 January 2019; Received in revised form 7 October 2019; Accepted 30 October 2019

involves the formation of a hierarchical structure or aerogel. TiO_2/SiO_2 aerogel has been reported to have excellent photocatalytic properties because the mesostructure can overcome intrinsic weaknesses, particularly in relation to the electron-transporting ability. Previous studies have provided data that confirm the intensive light harvesting demonstrated by TiO_2/SiO_2 with a mesoporous structure [11].

TiO_2/SiO_2 materials possess different performance properties depending on the mechanism of preparation and the synthetic route. Moreover, the porous structure of silica within the composite is also affected by various parameters, including the silica precursor. Silica prepared from plants or other biomass materials (termed biogenic silica) is increasingly used because of its renewable properties. Many attempts have been made to synthesize silica, silica nanoparticles, and mesoporous silica in the form of aerogels, hydrogels, etc. from a range of biomass materials, including rice husks, sugarcane bagasse, peanut shells, and other agricultural waste [9, 10]. According to existing studies on biogenic silica synthesis, a silica aerogel with a mesoporous structure is a possible option to enhance the performance of TiO_2/SiO_2 aerogel. Considering the proliferation of bamboo plants in Indonesia, this research proposes that bamboo leaves be used as a biogenic silica source in the preparation of TiO_2/SiO_2 materials. The utilization of bamboo leaves for silica aerogel formation has been discussed in the literature, but the characteristics of biogenic silica derived from these leaves have not been intensively studied.

Furthermore, the contribution of biogenic silica characteristics to the mechanism of TiO_2/SiO_2 formation, the specific mechanism involved, and investigation of the effects of synthetic parameters on the final physicochemical characteristics are of interest [12, 13]. Studies on the preparation of TiO_2/SiO_2 using biogenic silica from bamboo leaves have not been undertaken. According to other investigations, the physical performance of TiO_2/SiO_2 can be described based on such parameters as the specific surface area, crystallinity, and band gap energy as a result of specific preparation variables. As the performance activities of the TiO_2/SiO_2 materials in the photo-oxidation processes of organic molecules are significant in terms of their use as photocatalysts, such studies are important for the advancement of environmental technology.

The main objective in this study was to investigate the physicochemical characteristics of TiO_2/SiO_2 materials prepared using biogenic silica from bamboo leaves. These characteristics were measured as a function of preparation variables, such as Ti content, and calcination temperatures and their relationship with the photocatalytic activity performance were investigated.

2. Materials and methods

2.1. Materials

The reagent titanium tetraisopropoxide ($Ti(OiPr)_4$) was purchased from Sigma-Aldrich (Germany). Methylene blue (MB), H_2O_2, tetraethyl ortho silicate (TEOS) and acetic acid were obtained from Merck (Germany). Double distilled water was used in preparing the photocatalysts. All reagents were used without any further purification. Bamboo leaves were collected from *Gigantochloa apus* plants grown in the Sleman District, Yogyakarta, Indonesia. The leaves were washed with water and oven-dried before being calcined at 900 °C for 2 h to produce bamboo leaf ash (BLA).

2.2. SiO_2 extraction from BLA

SiO_2 extraction from BLA was performed by refluxing BLA with 4 M NaOH for 6 h. The reaction during the reflux is as follows:

$$SiO_2 + 2NaOH --> Na_2SiO_3 + H_2O$$

The slurry was then filtered, and the black residue was rinsed with boiling water. The viscous, transparent, and colorless filtrate had a pH of 13. The filtrate was cooled to room temperature, and slow titration was carried out by dropping in 1 M H_2SO_4 until white SiO_2 gel was obtained and the pH reached 8.

The gel was neutralized by adding double-distilled water several times to remove excess NaOH and sulphate ions, and was then decanted off before slow drying in an oven at 40 °C. To determine the silica content and surface profile of the compact white silica gel product, analyses were performed using a gravimetric method and scanning electron microscopy-energy dispersive X-ray spectrophotometry (SEM-EDX).

2.3. Preparation of TiO_2/SiO_2

TiO_2/SiO_2 composites were prepared using the silica present in the gel. A sol–gel method for the titania and silica reaction was used for the synthesis. As the TiO_2 precursor, $Ti(OiPr)_4$ was reacted with the SiO_2 obtained from the BLA extraction. In order to study the effect of the Ti content on the physicochemical properties of the composite, various Ti contents in the TiO_2/SiO_2 were obtained by changing the $Ti(OiPr)_4$ content in the sol–gel reaction. For each preparation, $Ti(Oipr)_4$ was diluted in 100 mL of ethanol, followed by the dropwise addition of 4 mL of acetic acid to initiate the hydrolysis reaction. Acetic acid was added to control TiO_2 hydrolysis, as described elsewhere [14, 15]. The mixture was then slowly mixed with the silica gel in water. For each reaction, the resulting colloidal solution was continuously stirred for one additional hour, followed by aging for 48 h at room temperature. The colloid was dried in an oven at 80 °C before being calcined at 500 °C. The mass percentage of TiO_2 in the composite was set to 20%, 30%, 40%, and 60%. The composites were encoded as $20TiO_2/SiO_2$, $30TiO_2/SiO_2$, $40TiO_2/SiO_2$, and $60TiO_2/SiO_2$, referring to the Ti content. As reference material, TiO_2 was prepared using a similar procedure and precursor as in the TiO_2/SiO_2 preparation but without mixing with silica gel.

2.4. Characterization

Powder X-ray diffraction (XRD) patterns of the samples were determined using a Shimadzu X6000 diffractometer (Tokyo, Japan) and Ni-filtered Cu Kα radiation operating at 30 mA and 40 kV. The diffraction data were collected using a continuous scan mode with a speed of 4°/min. Fourier transform infrared (FTIR) spectra of the samples were collected in the 400–4000 cm^{-1} region with a Perkin Elmer spectrometer (Singapore) using the KBr technique The surface morphologies of the samples were observed using SEM (JEOL, Tokyo, Japan). The specific surface areas (Brunauer-Emmett-Telle [BET] method), pore volumes, and pore radii (using Barret-Joyner-Hallenda/BJH method) of the samples were obtained by N_2 physisorption at 77 K using a Quantachrome apparatus (Singapore). All the samples were degassed at 150 °C prior to each analysis. A diffuse-reflectance UV-vis spectrophotometry (UV-DRS) instrument (JASCO V760, JASCO; Tokyo, Japan) was used in the range of 190–850 nm to determine the band gap energy (E_g) using $BaSO_4$ powder as a reference material. The E_g value was calculated using the Kubelka–Munk function (1):

$$F(R_\infty) = \frac{(1 - R_\infty)^2}{2R_\infty} \quad (1)$$

where R_∞ is the measured absolute reflectance of the sample ($R_{sample}/R_{standard}$) and E_g was calculated as the intercept from the plot of $(F(R\infty)\ h\nu)^{1/2}$ versus $h\nu$.

2.5. Photocatalytic activity evaluation

The evaluation of the photocatalytic performance of materials for the degradation of MB was performed on a reactor equipped with a UV lamp (Philips, 366 nm, 30 W) serving as the light source. Typically, 0.2 g of photocatalyst was added to 500 mL of MB solution (20 mg L^{-1}). Each mixture was previously stirred for 15 min in the dark before light

exposure to obtain absorption–desorption equilibrium before being subjected to light irradiation. MB photocatalytic degradation experiments were conducted both in the presence and absence of H_2O_2. For kinetics analyses, 2 mL of solution was sampled at certain time points of each experiment. The MB concentration was detected using a Hitachi U-2010 UV–vis spectrophotometer (Hitachi; Tokyo, Japan).

3. Results and discussion

3.1. Physicochemical characterization of materials

Fig. 1 shows SEM micrographs of BLA, SiO_2, and TiO_2/SiO_2 samples. EDX analysis data are listed in Table 1.The SEM results indicate that both the BLA and SiO_2 exhibited irregular shapes and seemed to have an amorphous structure. The EDX spectra of BLA and SiO_2 demonstrated the presence of SiO_2 as the dominant component, with 27.65% and 47.65%, respectively. Increasing the TiO_2 content in the samples led to the appearance of surface aggregates in the TiO_2/SiO_2 samples. The spherical forms may be ascribed to the formation of titanium dioxide. By comparing the TiO_2 contents, we found that a higher Ti content corresponded to larger aggregates on the surface.

Fig. 2 shows the comparison of the FTIR spectra of the SiO_2 and TiO_2/SiO_2 materials. Broad bands at 3430 cm^{-1} and 1630 cm^{-1} in both spectra corresponded to the stretching vibration and bending vibration of hydroxyl groups and surface adsorbed water, respectively. The TiO_2/SiO_2 sample exhibited characteristic peaks at 500 cm^{-1}, 1080 cm^{-1}, and 950

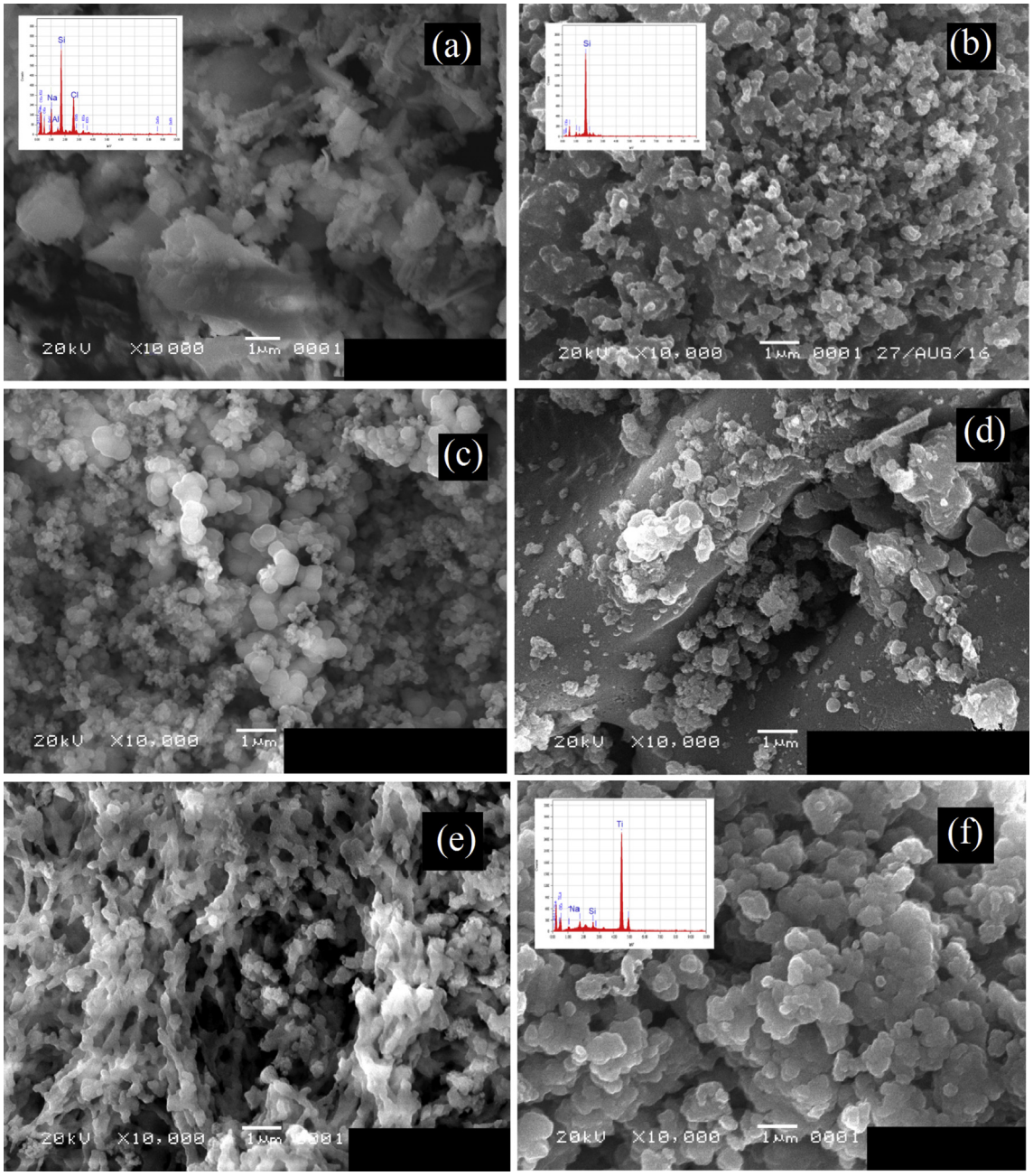

Fig. 1. SEM profile of (a) BLA (b) SiO_2 (c) $20TiO_2/SiO_2$ (d) $30TiO_2/SiO_2$, (e) $40TiO_2/SiO_2$, and (f) $60TiO_2/SiO_2$.

Table 1
Elemental analysis of BLA and TiO_2/SiO_2 samples.

Element (mass %)	BLA	SiO_2	$20TiO_2/SiO_2$	$30TiO_2/SiO_2$	$40TiO_2/SiO_2$	$60TiO_2/SiO_2$	TiO_2
O	47.53	42.53	48.3	46.56	32.72	39.47	42.77
Si	27.65	47.65	30.17	24.45	20.23	1.65	n.d
Na	3.56	3.56	1.07	0.68	7.03	1.37	n.d
Ti	n.d	n.d	18.88	27.89	39.9	55.80	57.23
C	20.03	5.03	0.56	0.34	n.d	n.d	n.d
Al	1.23	1.23	n.d	n.d	n.d	n.d	n.d
S	n.d	n.d	1.02	0.08	0.12	1.06	n.d
Total	100	100	100	100	100	100	100

nd: not detected.

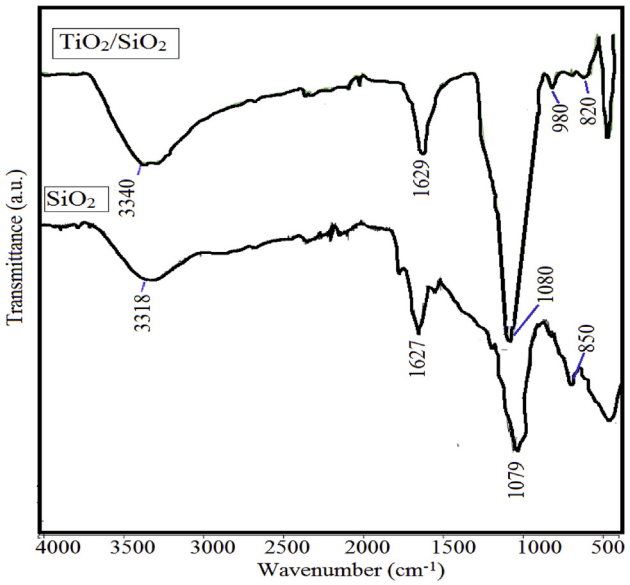

Fig. 2. FTIR spectra of SiO_2 and TiO_2/SiO_2.

cm^{-1} that are attributed to the stretching vibrations of Ti–O, Si–O–Si, and Ti–O–Si, respectively. The spectra at around 820–850 nm are attributed to the Si–O–Si and were demonstrated by both materials. The vibrations appear as indicators of the Ti–Si interaction at the molecular level [16].

Fig. 3 presents the XRD patterns of SiO_2 and TiO_2/SiO_2 samples. The patterns indicate that SiO_2 was present in the amorphous form, as characterized by a broad reflection at the 2θ of 22°. The synthesized

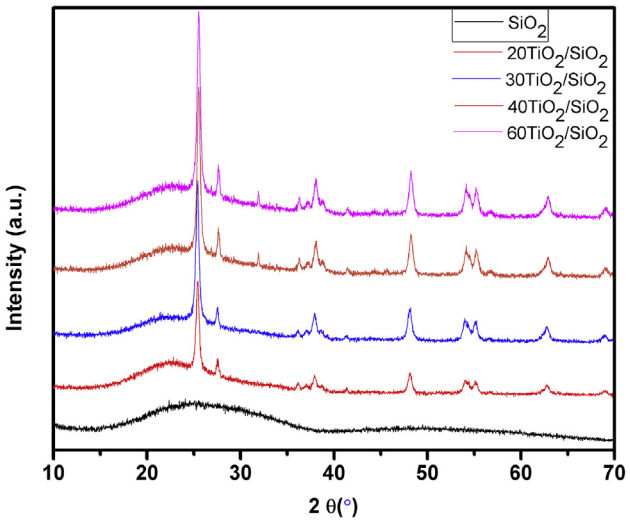

Fig. 3. XRD pattern of materials.

TiO_2/SiO_2 materials demonstrated similar phases, mainly consisting of TiO_2 anatase. The presence of anatase was identified by the reflections at 25.10°, 38.04°, 47.2°, and 62.5° (refer to JCPDS card no. 21–1272. From the pattern, it can be seen that only the anatase phase was present, while the rutile phase did not appear. Referring to previous works regarding the formation of TiO_2 and TiO_2–SiO_2, calcination temperatures in the range of 400 °C–600 °C tend to produce anatase crystals rather than rutile crystals, which are formed when the temperature exceeds 700 °C [17].

The grain size in the anatase phase was calculated from the full width at half maxima (FWHM) of the peaks at 25.1° and 38.01° using Scherrer's Eq. (2):

$$Lc = \frac{K\lambda}{\beta \cos \theta} \quad (2)$$

where λ is the X-ray wavelength, β is the FWHM of the diffraction line, θ is the diffraction angle, and K is a constant that has been assumed to be 0.9. The data are presented in Table 2. The crystallite size depends on the TiO_2 content in the composite, and the average particle diameter increased with increasing TiO_2. These results are in good agreement with those reported by previous studies on the synthesis of SiO_2/TiO_2 [18, 19, 20]. A higher TiO_2 content in the synthesis causes the particle size of the aggregates to increase as a consequence of the larger size of the pre-formed TiO_2 nanoparticles during the sol–gel transition [16].

The microstructural properties of the materials were investigated using N_2 adsorption–desorption isotherms at 77 K Fig. 4 shows the adsorption–desorption isotherms and Barrett–Joyner–Halenda (BJH) pore distributions from the desorption profiles of SiO_2 and TiO_2/SiO_2 samples. The pure SiO_2 material exhibited an isotherm related to non-porous material, while the TiO_2/SiO_2 samples exhibited a type IV isotherm, characteristic of the combination of microporous and mesoporous materials.

The adsorbed amount of N_2 molecules at low relative pressures increased with TiO_2 content. The surface area, pore volume, and average pore radius calculated are listed in Table 2. The BET-specific surface area and BJH pore diameter results suggest that increasing the TiO_2 content from 0% to 40% leads to improvements in the specific surface area and pore volume. However, the average pore size decreased due to the

Table 2
Surface area, pore volume and pore radius of materials.

Sample	BET specific surface area (m^2/g)	Pore Volume (cc)	Pore Radius (Å)	TiO_2 crystallite size (nm)
SiO_2	20.98	2.30×10^{-2}	102.2	0
$20TiO_2/SiO_2$	55.45	5.23×10^{-2}	93.4	6.44
$30TiO_2/SiO_2$	124.04	1.95×10^{-1}	35.7	6.86
$40TiO_2/SiO_2$	165.16	3.62×10^{-1}	38.2	9.05
$60TiO_2/SiO_2$	289.23	4.02×10^{-1}	29.43	13.08
TiO_2	135.23	2.21×10^{-1}	35.6	11.5

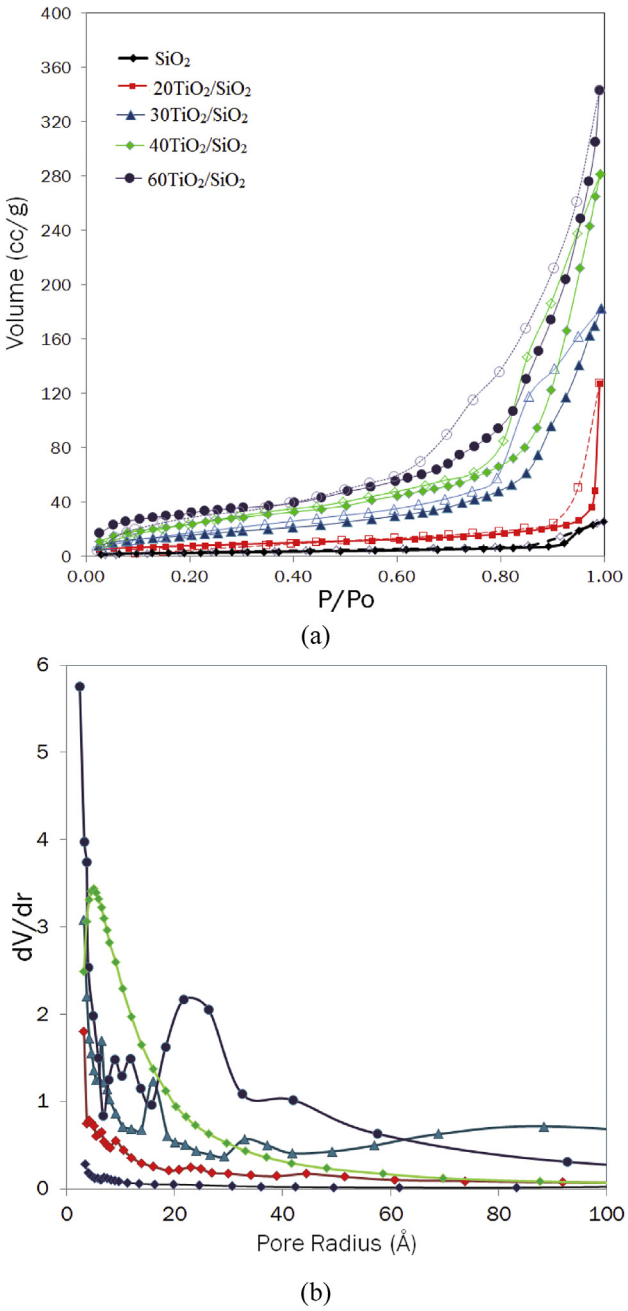

Fig. 4. (a) Adsorption-desorption profile and (b) BJH-pore distribution of materials.

formation of different pores. From the pore distributions, it can be noted that the composites exhibited different features than the pure SiO_2 due to the presence of TiO_2 species, and their shapes depended on the TiO_2 content. The formation of larger pore diameters was achieved for the 60-TiO_2/SiO_2 sample, resulting in larger aggregates of TiO_2 for higher TiO_2 amounts in the TiO_2/SiO_2 material.

The band gap energy of TiO_2/SiO_2 was also affected by the TiO_2 content. The band gap energy is theoretically related to the particle size of a semiconductor. Diffuse reflectance spectra (DRS) in the UV-vis interval were analyzed to estimate the band gap of the samples. Plots of the band gap energy of TiO_2/SiO_2 materials as well as the calculated band gap energy are depicted in Fig. 5. The increase of the Ti content in the composite led to the enhanced band gap energy, and it reached a maximum at 3.22 eV for $40TiO_2/SiO_2$ and $60TiO_2/SiO_2$ (Fig. 5). The values did not vary linearly with the quantum size effect, which means

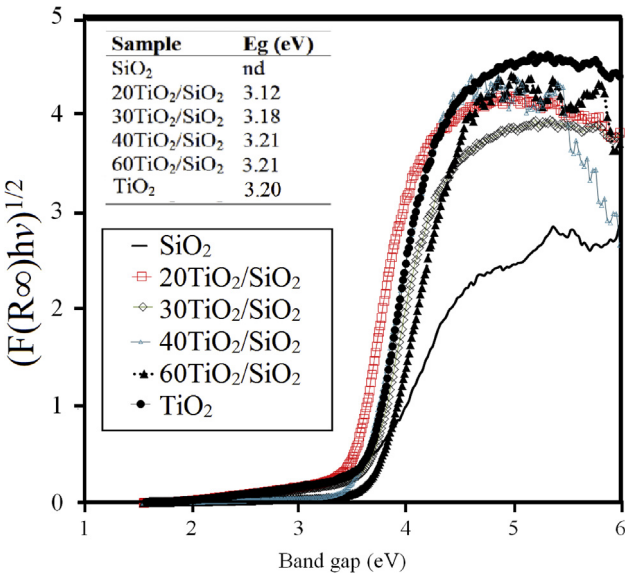

Fig. 5. DRS spectra of materials.

that a smaller particle size reflects increasing band gap energy [16]. The reason for this inconsistency is possibly related to the non-homogeneous distribution of TiO_2 particles on the SiO_2 surface.

3.2. Photocatalytic activity

The photocatalytic performances of the prepared materials were assessed based on room temperature MB photocatalytic degradation in the absence and presence of H_2O_2 as an additional oxidant. TiO_2 is photoactive material, and because a photon impinges on the semiconductor photocatalyst there will be an excitation of electrons from the valence band to the conductance band. This process leaves holes (h^+) that then will interact with solvent or hydroxyl ions in the system to form radicals. The presence of H_2O_2 contributes to the more rapid formation of •OH radicals in the system and leads to the faster oxidation of organic compounds. The mechanism is as follows:

$$TiO_2(e^-) + H_2O_2 \rightarrow TiO_2 + OH^- + \bullet OH$$

$$\bullet OH + O_2 \rightarrow \bullet O_2^- + H^+$$

$$H_2O_2 + \bullet O_2^- \rightarrow \bullet OH + OH^- + O_2.$$

The experiments involved a typical MB photocatalytic degradation experiment; 0.25 g L^{-1} of catalyst was added to 500 mL of an aqueous solution of MB, which was placed in the solution chamber supported with a 20 W UV lamp as the photon source. Before light irradiation, the suspension was stirred magnetically for 15 min to develop adsorption–desorption equilibrium. Sampling was performed at certain times, and the treated solution was analyzed using a spectrophotometric method.

Fig. 6 shows the kinetic patterns of MB photocatalytic degradation of materials in the absence and presence of H_2O_2. The kinetic patterns are also compared with the illumination without the addition of any photocatalyst. It is seen that the presence of all TiO_2/SiO_2 materials plays a role in MB decolorization, as there is no significant change in MB concentration with only UV light and no photocatalyst. The photocatalysis mechanism is also confirmed by a faster decolorization slope in the presence of UV light compared with pre-treatment without UV light illumination, which means that only adsorption takes place.

Five kinetic models were used to analyze the kinetic data relating to the photocatalytic degradation of MB on TiO_2/SiO_2 samples. The pseudo-zero-order model describes the degradation process and can be generally expressed as (3):

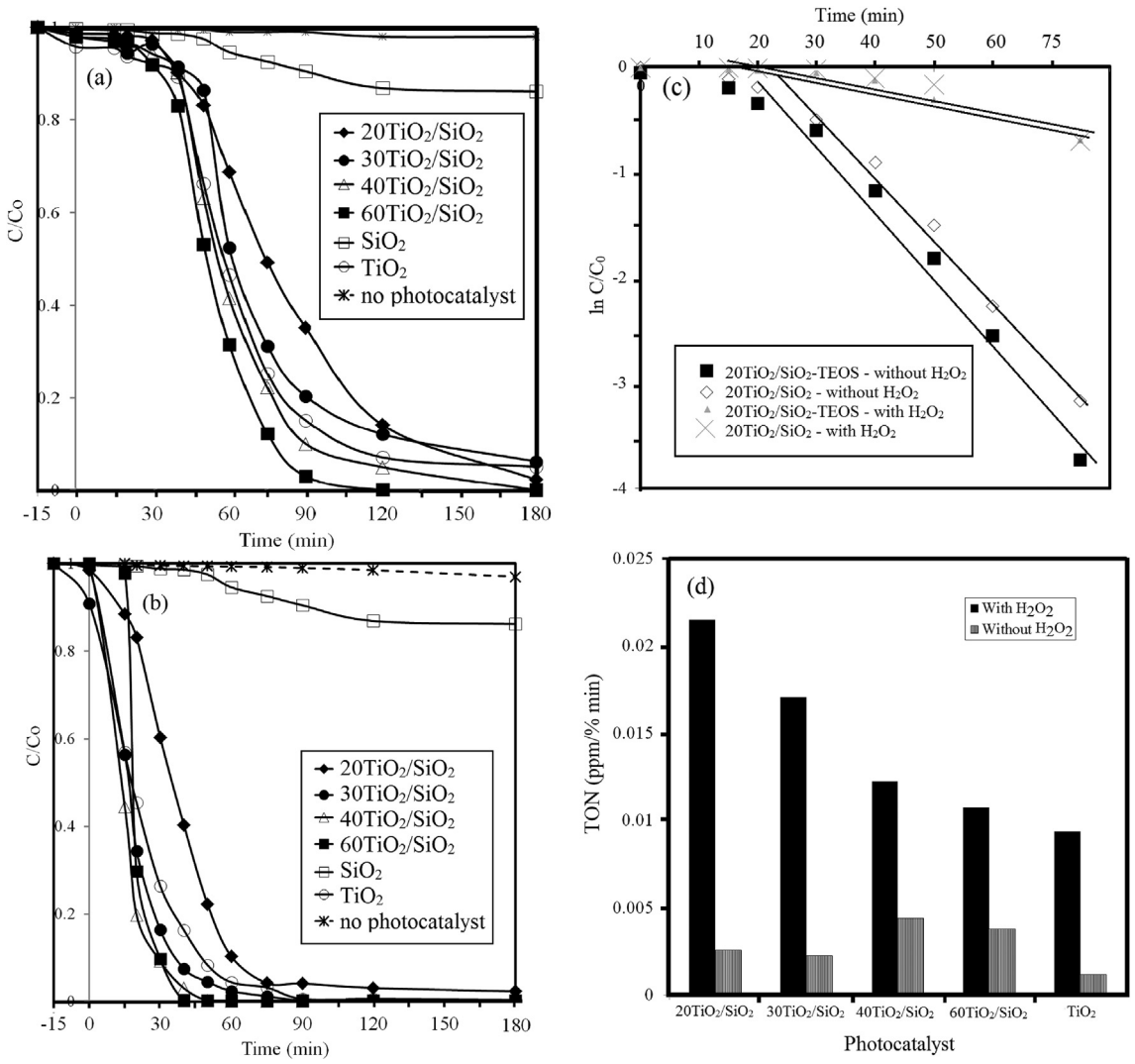

Fig. 6. (a) Kinetics of MB photocatalytic degradation without H_2O_2 addition (b) Kinetics of MB photocatalytic degradation with H_2O_2 addition (c) pseudo-first order plot of MB photocatalytic degradation using $20TiO_2/SiO_2$ and $20TiO_2/SiO_2$-TEOS (d) TON of photocatalytic degradation over varied photocatalysts.

$$C_o - C_t = kt \tag{3}$$

The pseudo-first-order model can be expressed as (4):

$$ln\left(\frac{C_0}{C_t}\right) = -kt \tag{4}$$

The pseudo-second-order model can be expressed as (5):

$$\left(\frac{1}{C_t} - \frac{1}{C_o}\right) = kt \tag{5}$$

The parabolic diffusion model can be expressed as (6):

$$\frac{\left(1 - C_t/C_0\right)}{t} = kt^{1/2} + \propto \tag{6}$$

The modified Freundlich model can be expressed as (7):

$$\frac{C_0 - C_t}{C_0} = kt^b \tag{7}$$

In these equations, C_0 and C_t are the concentrations of dye molecules in the solution at times 0 and t, respectively; k is the corresponding rate constant; α is the kinetic order of the parabolic diffusion model; and b is the Freundlich constant. The fitting of the kinetic data to various models and their corresponding coefficients of determination (R^2) are listed in Table 3.

We found that in the absence of H_2O_2, the photocatalytic degradation of MB over SiO_2 obeys pseudo-zero-order kinetics, while the kinetic data for the TiO_2/SiO_2 samples and TiO_2 are well fitted to pseudo-first order kinetics. This suggests that the rate of MB degradation over TiO_2/SiO_2 samples depends on the amount of dye molecules in the solution, while the MB degradation over SiO_2 is mainly affected by the adsorption process.

The addition of H_2O_2 in the reaction system catalyzed by $40TiO_2/SiO_2$ and $60TiO_2/SiO_2$ changes the kinetic models. The MB photocatalytic degradation over TiO_2/SiO_2 catalysts in the absence of H_2O_2 obeys pseudo-first-order kinetics; the same is true for the MB photocatalytic degradation over $20TiO_2/SiO_2$ and $30TiO_2/SiO_2$ with the addition of H_2O_2. Meanwhile, the reaction over $40TiO_2/SiO_2$ and $60TiO_2/SiO_2$ with the presence of H_2O_2 is more accurately fitted to the modified Freundlich model. The pseudo-first-order mechanism is based on the assumption that the rate-limiting step is the chemical sorption of MB as target molecules and that the oxidation occurs through photo-induced electron transfer between the reactants and photoactive particles [21, 22]. With the modified Freundlich model, the reaction is controlled by heterogeneous diffusion from the photocatalyst surface interaction among reactants. This suggests that the system is controlled

Table 3
Kinetics models and parameters of MB degradation by photocatalysis and photooxidation using materials.

Photocatalytic degradation	Condition	Kinetics model	Equation (R^2)	Initial rate (ppm/min)	Kinetics constant
SiO_2	Without H_2O_2	Pseudo-zero order	C_o-$C_t = 6.61.10^{-3}t$ (0.9587)	$4.85.10^{-2}$	$6.61.10^{-3}$
$20TiO_2/SiO_2$	Without H_2O_2	Pseudo-first order	ln (Co/Ct) = $-6.96.10^{-3}t$ (0.9566)	4.79. 10^{-2}	$6.96.10^{-3}$
$30TiO_2/SiO_2$	Without H_2O_2	Pseudo-first order	ln (Co/Ct) = $-7.81.10^{-3}t$ (0.9344)	6.25. 10^{-2}	$1.79.10^{-2}$
$40TiO_2/SiO_2$	Without H_2O_2	Pseudo-first order	ln (Co/Ct) = $-2.53.10^{-2}t+ 0.480$ (0.9645)	0.175	$2.53.10^{-2}$
$60TiO_2/SiO_2$	Without H_2O_2	Pseudo-first order	ln (Co/Ct) = $-3.74.10^{-2}t+ 0.717$ (0.9645)	0.209	$3.74.10^{-2}$
TiO_2	Without H_2O_2	Pseudo-first order	ln (Co/Ct) = $-2.12.10^{-2}t+ 0.363$ (0.9453)	6.45. 10^{-2}	$2.12.10^{-2}$
SiO_2	With H_2O_2	Pseudo-zero order	(C_o-$C_t = 6.62.10^{-3}t$ (0.9655)	$4.85.10^{-2}$	$6.61.10^{-3}$
$20TiO_2/SiO_2$	With H_2O_2	Pseudo-first order	ln (Co/Ct) = $-0.042.10^{-2}t+ 0.4676$ (0.9732)	0.405	$4.2.10^{-2}$
$30TiO_2/SiO_2$	With H_2O_2	Pseudo-first order	ln (Co/Ct) = $-0.064.10^{-2}t+ 0.1197$ (0.9956)	0.475	$6.30.10^{-2}$
$40TiO_2/SiO_2$	With H_2O_2	Modified-Freundlich model	($1-C_t/C_o$) = $-1.527t^{2.30}$ (0.9954)	0.488	0.235
$60TiO_2/SiO_2$	With H_2O_2	Modified- Freundlich model	($1-C_t/C_o$) = $-0.822t^{3.91}$ (0.9954)	0.599	0.374
TiO_2	With H_2O_2	Pseudo-first order	ln (Co/Ct) = $-2.52.10^{-2}t+ 0.164$ (0.9453)	0.525	$5.3.10^{-2}$

by the adsorption–desorption mechanism and that the degradation of the dye molecules occurs on the photocatalyst surface before being desorbed from the surface patches. This change refers to the higher specific surface area of $40TiO_2/SiO_2$ and $60TiO_2/SiO_2$ compared with $20TiO_2/SiO_2$ and $30TiO_2/SiO_2$, which potentially provide a larger active surface to adsorb MB and H_2O_2. The combination of higher specific surface area and band gap energy accelerates degradation by the more stable radicals formed, as there is an interaction between the photon and the photocatalyst. This assumption is strengthened by the degradation reactions over TiO_2 in the absence and presence of H_2O_2, which obey pseudo-first-order kinetics. The result is a lower initial rate compared with $40TiO_2/SiO_2$ and $60TiO_2/SiO_2$. Based on the kinetics constant and initial rate values, the photocatalytic activity of TiO_2 is in between that of $40TiO_2/SiO_2$ and $40TiO_2/SiO_2$. This suggests that based on TiO_2 content, the composite of TiO_2/SiO_2 enhances the photocatalytic efficiency, while the lower TiO_2 content in $40TiO_2/SiO_2$ and $60TiO_2/SiO_2$ results in a higher degradation rate.

In the perspective of utilization of Bamboo leaves ash as SiO_2 source, the comparison was also conducted with the use of $20TiO_2/SiO_2$ synthesized using TEOS as SiO_2 precursor (designated as $20TiO_2/SiO_2$-TEOS) with the physicochemical character data presented in Table 4. Based on the kinetics plots presented in Fig. 7, pseudo-first order plot (Fig. 6c) suggests that there is no significant different photocatalytic activity represented by the insignificant difference in kinetics constants the presence and absence of H_2O_2. The kinetics constants for photocatalytic degradation without H_2O_2 over $20TiO_2/SiO_2$ and $20TiO_2/SiO_2$-TEOS are 5.6×10^{-3}/min and 6.0×10^{-3}/min, meanwhile in the presence of H_2O_2, the constants are 4.2×10^{-2}/min and 4.6×10^{-2}/min, respectively. The higher values are corresponding to higher specific surface area. The role of composite formation of TiO_2 with SiO_2 can be evaluated by the turnover numer (TON) which calculated by following equation:

$$TON = \frac{Initial\ rate\ \left(\frac{ppm}{\min}\right)}{Ti(\%)} \quad (8)$$

The data depicted in Fig. 6d represents that all TiO_2/SiO_2 samples demonstrated higher values compared with TiO_2 for the photocatalytic degradation by both with H_2O_2 and without H_2O_2 addition. It means that as photoactive material, the photocatalytic activity of TiO_2 in support formation tends to be more effective in composite form.

The occurrence of faster oxidation in the presence of an oxidant is proven by the spectrophotometric spectra of the treated solutions in Fig. 8. The faster reduction of the MB maximum wavelength and the hypsochromic shifts throughout the time of treatment are ascribed to the chemical change of the MB structure. The change in the UV-vis spectrum

Table 4
Physicochemical character of $20TiO_2/SiO_2$-TEOS.

Parameter	Value
Element (mass %)	
O	47.89
Si	32.31
Ti	19.80
Specific surface area (m^2/g)	76.15
Pore Volume (cc/g)	52.70
Band Gap Energy (eV)	3.18

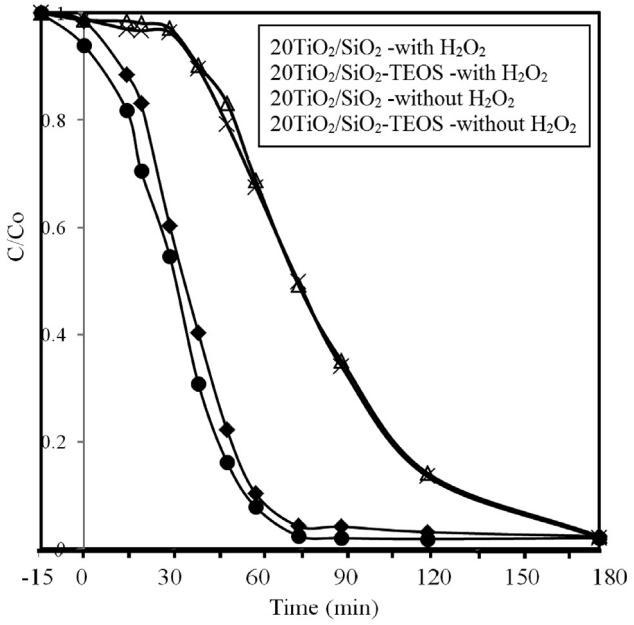

Fig. 7. Kinetics of photocatalytic degradation by $20TiO_2/SiO_2$ and $20TiO_2/SiO_2$-TEOS.

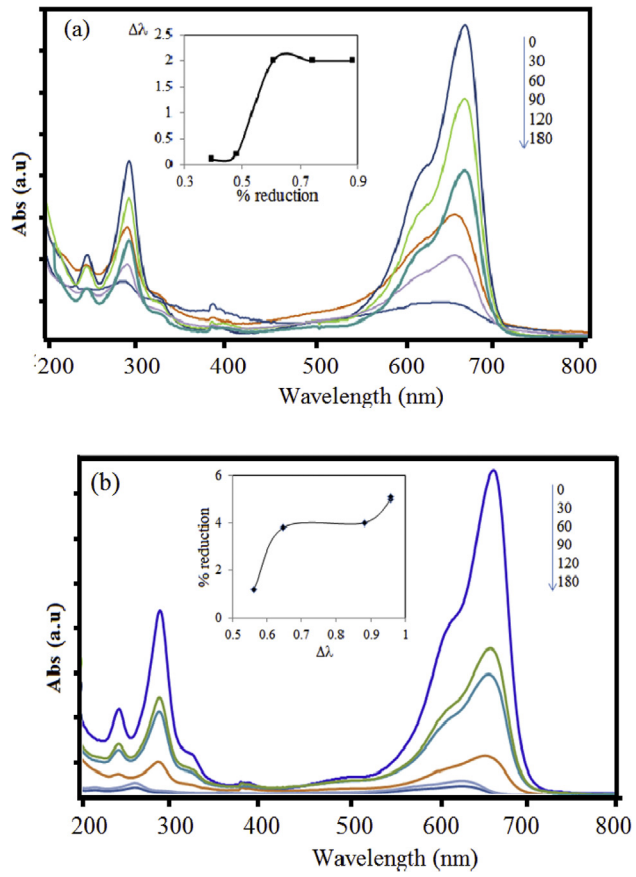

Fig. 8. UV-Vis spectra of treated MB solution by photocatalytic degradation (a) without H_2O_2 addition (b) without H_2O_2 addition.

due to the photo-oxidation mechanism depicts the result of the N-demethylation of the dimethylamine group in MB [23, 24]. The values of the initial rate suggest that the presence of H_2O_2 enhances the degradation rate by twice that with respect to its absence. The more rapid MB degradation with the increasing Ti content is related to the more rapid formation of radicals with increasing holes and solvent and H_2O_2 interaction during the mechanism. Overall, it is about 99% of the MB degradation reached at about 40 min by all TiO_2/SiO_2 photocatalyst samples under photo-oxidation mechanisms. Meanwhile, similar degradation percentage values are reached at around 120 min via the photocatalysis mechanism. This is also assumed based on the higher band gap energy for the higher Ti content and the larger specific surface area and pore volume in the TiO_2/SiO_2 materials.

4. Conclusion

A series of TiO_2/SiO_2 composites using biogenic silica from bamboo leaves as the silica source and titanium isopropoxide were synthesized using a sol-gel process. The materials showed physicochemical characteristics to be functional as photocatalysts. TiO_2 in anatase phase is found in all varied TiO_2 content. It is also noted that in the range of 20–60% wt. varied TiO_2 percentage in the preparation, the higher TiO_2 content helps to increase particle size in the anatase phase and to increase specific surface area, pore distribution, and band gap energy (E_g). These physicohemical properties have an important role in the photocatalysis mechanism. The presence of H_2O_2, higher specific surface area, and higher band gap energy are prominent factors that accelerate the degradation mechanism. The notifiable data is that kinetics of photocatalytic degradation over $40TiO_2/SiO_2$ and $60TiO_2/SiO_2$ with the addition of H_2O_2 obey the modified Freundlich kinetic model, while other photocatalytic degradation using TiO_2/SiO_2 samples obeys pseudo-first-order kinetics.

Declarations

Author contribution statement

Is Fatimah: Conceived and designed the experiments; Performed the experiments; Analyzed and interpreted the data; Contributed reagents, materials, analysis tools or data; Wrote the paper.

Nurcahyo Iman Prakoso: Performed the experiments.

Imam Sahroni, Muhammad Miqdam Musawwa: Performed the experiments; Analyzed and interpreted the data.

Yoke-Leng Sim, Fethi Kooli, Oki Muraza: Analyzed and interpreted the data; Contributed reagents, materials, analysis tools or data; Wrote the paper.

Funding statement

This work was supported by the Indonesia Toray Science Foundation (ITSF), Indonesia and World Class Research grant from Kemenristek-DIKTI, Republic of Indonesia.

Competing interest statement

The authors declare no conflict of interest.

Additional information

No additional information is available for this paper.

References

[1] Y. Chen, K. Wang, L. Lou, Photodegradation of dye pollutants on silica gel supported TiO_2 particles under visible light irradiation, J. Photochem. Photobiol. A: Chem. 163 (2004) 281–287.

[2] L. Lin, Y. Chai, B. Zhao, W. Wei, D. He, B. He, et al., Photocatalytic oxidation for degradation of VOCs, Open J. Inorg. Chem. 3 (2013) 14–25.

[3] J. Herrmann, C. Duchamp, M. Karkmaz, B.T. Hoai, H. Lachheb, E. Puzenat, et al., Environmental green chemistry as defined by photocatalysis, J. Hazard Mater. 146 (2007) 624–629.

[4] P.A. Pekakis, N.P. Xekoukoulotakis, D.M. Ã, Treatment of textile dyehouse wastewater by TiO_2 photocatalysis, J. Water Res. 40 (2006) 1276–1286.

[5] J. Šíma, P. Hasal, Photocatalytic degradation of textile dyes in a TiO_2/UV system, Chem. Eng. Trans. 32 (2013) 79–84.

[6] K. Hashimoto, H. Irie, A. Fujishima, TiO_2 photocatalysis: a historical overview and future prospects, Jpn. J. Appl. Phys. 44 (2005) 8269–8285.

[7] P. Sun, J. Zhang, W. Liu, Q. Wang, W. Cao, Modification to L-H kinetics model and its application in the investigation on photodegradation of gaseous benzene by nitrogen-doped TiO_2, Catalysts 8 (2018) 326.

[8] F.A. Harraz, O.E. Abdel-Salam, A.A. Mostafa, R.M. Mohamed, M. Hanafy, Rapid synthesis of titania–silica nanoparticles photocatalyst by a modified sol–gel method for cyanide degradation and heavy metals removal, J. Alloys Comp. 551 (2013) 1–7.

[9] J.M. Rankin, S. Baker, K.J. Klabunde, Mesoporous aerogel titanium oxide-silicon oxide combinations as adsorbents for an azo-dye, Micro. Meso. Mater. 190 (2014) 105–108.

[10] M.A. Camblor, M. Constantini, A. Corma, P. Esteve, L. Gilbert, A. Martinez, et al., A new highly efficient method for the synthesis of Ti-Beta zeolite oxidation catalyst, Appl. Catal. A, General 133 (1995) 0–4.

[11] X.-D. Gao, X.-M. Li, X.-Y. Gan, Y.-Q. Wu, R.-K. Zheng, C.-L. Wang, et al., Aerogel based SiO_2–TiO_2 hybrid photoanodes for enhanced light harvesting in dye-sensitized solar cells, J. Mater. Chem. 22 (2012) 18930.

[12] H.L. Wang, W.Z. Liang, W.F. Jiang, Solar photocatalytic degradation of 2-sec-butyl-4,6-dinitrophenol (DNBP) using TiO_2/SiO_2 aerogel composite photocatalysts, Mater. Chem. Phys. 130 (2011) 1372–1379.

[13] G.N. Shao, Y. Kim, S.M. Imran, S.J. Jeon, P.B. Sarawade, A. Hilonga, et al., Enhancement of porosity of sodium silicate and titanium oxychloride based TiO_2-SiO_2 systems synthesized by sol-gel process and their photocatalytic activity, Micro. Meso. Mater. 179 (2013) 111–121.

[14] R.F.S. Lenza, W.L. Vasconcelos, Synthesis of titania-silica materials by sol-gel, Mater. Res. 5 (2002) 497–502.

[15] R.A. Aziz, N. Asyikin, I. Sopyan, Synthesis of TiO_2-SiO_2 powder photocatalyst via sol-gel method: effect of titanium precursor type on powder properties, J. Inst. Eng., Malaysia 70 (2009) 34–40.

[16] L. Pinho, M.J. Mosquera, Photocatalytic activity of TiO_2-SiO_2 nanocomposites applied to buildings: influence of particle size and loading, Appl. Catal. B: Environ. 134–135 (2013) 205–221.
[17] J. Zhai, L. Zhang, X. Yao, Effects of composition and temperature on gel-formed TiO_2/SiO_2 films, J. Non-Cryst. Solids 260 (1999) 160–163.
[18] S. Ren, X. Zhao, L. Zhao, M. Yuan, Y. Yu, Y. Guo, et al., Preparation of porous TiO2/silica composites without any surfactants, J. Solid State Chem. 182 (2009) 312–316.
[19] J.-X. Liu, F. Shi, L.-N. Bai, X. Feng, X.-K. Wang, L. Bao, Synthesis of TiO_2–SiO_2 aerogel via ambient pressure drying: effects of sol pre-modification on the microstructure and pore characteristics, J. Sol-Gel Sci. Technol. 69 (2014) 93–101.
[20] H. Chun, W. Yizhong, T. Hongxiao, Preparation and characterization of surface bond-conjugated TiO_2/SiO_2 and photocatalysis for azo dyes, Appl. Catal. B: Environ. 30 (2001) 277–285.
[21] I. Fatimah, S. Fadillah, Yulan, TiO_2 supported on brick waste as low cost photocatalyst for dye photodegradation, Chem. Eng. Trans. 63 (2018).
[22] Q. Sun, X. Hu, S. Zheng, Z. Sun, S. Liu, H. Li, Influence of calcination temperature on the structural, adsorption and photocatalytic properties of TiO_2 nanoparticles supported on natural zeolite, Powder Technol. 274 (2015) 88–97.
[23] T. Zhang, T. Oyama, S. Horikoshi, H. Hidaka, J. Zhao, N. Serpone, Photocatalyzed N-demethylation and degradation of methylene blue in titania dispersions exposed to concentrated sunlight, Sol. Energy Mater. Sol. Cells 73 (2002) 287–303.
[24] T. Zhang, T. Oyama, A. Aoshima, H. Hidaka, J. Zhao, N. Serpone, Photooxidative N-demethylation of methylene blue in aqueous TiO_2 dispersions under UV irradiation, J. Photochem. Photobiol. A: Chem. 140 (2001) 163–172.